CMS Physics Analysis Summary

Contact: cms-pag-conveners-higgs@cern.ch 2016/08/05

Search for Higgs boson pair production in the $\mathrm{b\bar{b}l\nu l\nu}$ final state at $\sqrt{s} = 13$ TeV

The CMS Collaboration

Abstract

A search for pair-produced Higgs bosons decaying respectively into $\mathrm{b\bar{b}}$ and VV (with V either a W or a Z boson), with subsequent VV decays into two leptons and two neutrinos, is presented. The analysis is based on a sample of proton-proton collisions at $\sqrt{s} = 13$ TeV at the LHC corresponding to an integrated luminosity of 2.30 fb^{-1}. The search signature is a resonance in the invariant mass distribution of the b-jet pair at the Higgs boson mass in combination with high scores of a boosted decision tree discriminant based on kinematic information. Data and predictions from the standard model (SM) are in agreement within uncertainties. For the SM hh hypothesis, the data are observed (expected) to exclude a production cross-section times branching ratio of 166.7 ($92.8^{+59.9}_{-33.4}$) fb, corresponding to approximately 400 times the SM cross section. Lack of deviation from the SM predictions in the observations is used to place constraints on different scenarios considering anomalous couplings which could affect the rate and kinematics of hh production.

1 Introduction

The Brout-Englert-Higgs mechanism is an essential element of the standard model (SM) of particles and their interactions explaining the origin of mass and playing a key role in electroweak symmetry breaking [1–6]. The discovery of a Higgs boson with a mass of around 125 GeV by the ATLAS and CMS experiments [7, 8] fixes the value of the self-coupling in the scalar potential whose form is determined by the symmetries of the SM and the requirement of renormalisability. Direct information on the Higgs three- and four-point interactions could provide a indication of the scalar potential structure.

To answer some of these questions, Higgs boson pair production, sensitive to the self-coupling λ, will play a major role. At the LHC, Higgs boson pairs are predominantly produced through gluon fusion via two diagrams (Fig. 1 top). In the SM the destructive interference between these two diagrams makes the measurement of Higgs boson pair production extremely challenging, even in most optimistic scenarios in terms of energy and integrated luminosity at the future HL-LHC. The SM cross section for hh production at 13 TeV is $\sigma^{\mathrm{hh}}_{\mathrm{NNLO}} = 33.45$ fb [9–18].

New physics coming from Beyond the Standard Model (BSM) phenomena has not been observed at the LHC, in either direct searches or precision measurements. This evidence suggests the existence of a gap between the electroweak scale and the new physics scale. Indirect effects at the electroweak scale due to BSM phenomena at a higher scale can be parametrized in an effective field theory framework [19–21], leading to deviations of the SM parameters involved in Higgs pair (hh) production, namely the Higgs boson self-coupling λ (coupling modifier $\kappa_\lambda = \frac{\lambda}{\lambda_{\mathrm{SM}}}$) and the top quark Yukawa coupling y_{t} (coupling modifier $\kappa_{\mathrm{t}} = \frac{y_{\mathrm{t}}}{y_{\mathrm{t_{SM}}}}$), and to the appearance of new contact-like interactions, of the Higgs boson with gluons (c_{g}), Higgs boson pair with a gluon pair ($c_{2\mathrm{g}}$) and Higgs boson pair with a top quark pair (c_2) (Fig. 1 bottom). Such modifications of the Higgs couplings would enhance Higgs boson pair production, opening the possibility of a BSM discovery before observation of SM hh. The relevant part of the modified Lagrangian takes the form:

$$\mathcal{L}_h = \frac{1}{2}\partial_\mu h \partial^\mu h - \frac{1}{2}m_h^2 h^2 - \kappa_\lambda \lambda_{SM} v h^3 - \frac{m_t}{v}(v + \kappa_t h + \frac{c_2}{v} h h)(\bar{t_L} t_R + h.c.) + \frac{1}{4}\frac{\alpha_s}{3\pi v}(c_g h - \frac{c_{2g}}{2v} h h) G^{\mu\nu} G_{\mu\nu} . \quad (1)$$

Searches for Higgs pair production have been performed by the ATLAS and CMS experiments using LHC proton-proton collision data. These include searches for BSM production in $\sqrt{s} =$ 8 TeV data [22] and $\sqrt{s} = 13$ TeV data [23], as well as more targeted searches for production with SM-like kinematics in $\sqrt{s} = 8$ TeV data [24–27] and $\sqrt{s} = 13$ TeV data [28, 29].

In this document we report on a search for Higgs pair production, hh, where one of the h decays as $\mathrm{h} \to \mathrm{b\bar{b}}$, and the other as $\mathrm{h} \to \mathrm{VV} \to \mathrm{l\nu l\nu}$ (where V is either a W or a Z boson, and l is either an electron or a muon) using LHC proton-proton collision data at $\sqrt{s} = 13$ TeV. The analysis focuses on the invariant mass distribution of the b-jet pair, searching for a resonant-like excess compatible with the h boson mass in combination with a boosted decision tree discriminant based on kinematic information. The dominant background is $\mathrm{t\bar{t}}$ production, with smaller contributions from Drell-Yan+jets and single top production. Figure 1 shows the Higgs pair production diagrams via gluon fusion.

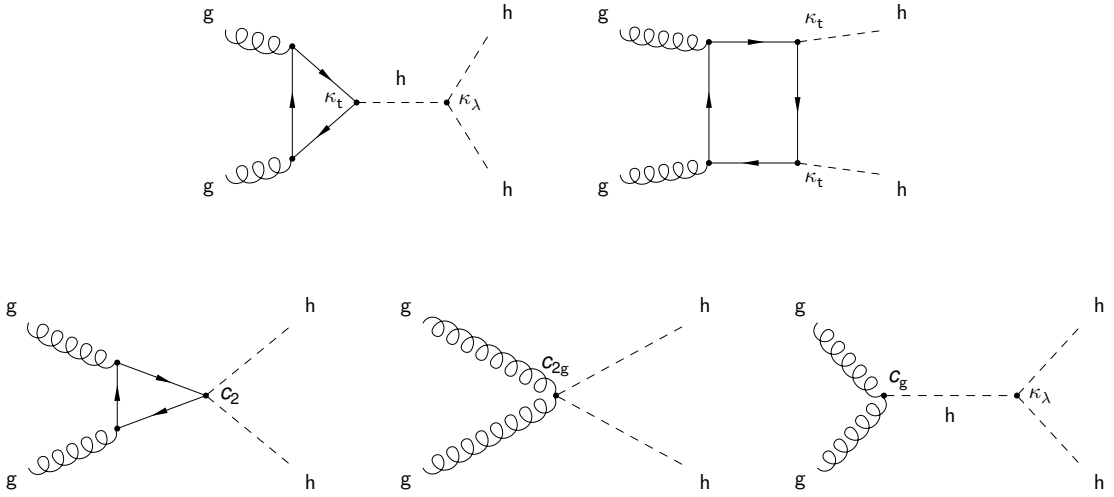

Figure 1: Higgs pair production diagrams via gluon fusion for both SM (top) and BSM (bottom).

2 The CMS detector and simulation

The central feature of the CMS apparatus is a superconducting solenoid of 6 m internal diameter, providing a magnetic field of 3.8 T. Within the superconducting solenoid volume are a silicon pixel and strip tracker, a lead tungstate crystal electromagnetic calorimeter (ECAL), and a brass and scintillator hadron calorimeter (HCAL), each composed of a barrel and two endcap sections. Forward calorimeters extend the pseudorapidity coverage provided by the barrel and endcap detectors. Muons are measured in gas-ionization detectors embedded in the steel flux-return yoke outside the solenoid. A more detailed description of the CMS detector, together with a definition of the coordinate system used and the relevant kinematic variables, can be found in Ref. [30].

The main background processes, in order of decreasing expected yields, are: $\mathrm{t\bar{t}}$, Drell-Yan, and single top. Diboson production, $\mathrm{t\bar{t}V}$ production, as well as single SM Higgs production with subsequent decays $\mathrm{h} \to \mathrm{VV}$ and $\mathrm{h} \to \mathrm{b\bar{b}}$, are also taken into account in the analysis even if they do not contribute in a visible way. Other contributions, such as W + jets or QCD multijet events with jets misidentified as leptons, are negligible due to the tight dilepton selection. The dominant contribution, especially in the $\mathrm{e}^{\pm}\mu^{\mp}$ selection, arises from $\mathrm{t\bar{t}}$ production yielding the same final state (2 b-jets, 2 leptons, and 2 neutrinos) when both W bosons decay as $\mathrm{W} \to \mathrm{l}\nu$. Background contributions are estimated directly from simulation.

Background simulation samples have been generated using MADGRAPH 5 versions 2.2.2.0 and 2.3.2.2 [31], POWHEG 2 [32–36] and PYTHIA 8 [37, 38] version 8.205. The signal samples have been generated using MADGRAPH 5 version 2.2.2.0 and describe events at leading order of gluon fusion production of two SM-Higgs bosons with a mass of 125 GeV. One of the Higgs boson is required to decay into a pair of b-quarks, while the second one is required to decay to final states containing two leptons and two neutrinos. This implies that the signal samples contain both $\mathrm{h} \to \mathrm{Z(ll)Z}(\nu\nu)$ and $\mathrm{h} \to \mathrm{W(l}\nu\mathrm{)W(l}\nu\mathrm{)}$ decay legs. The SM branching ratios are assumed, therefore the interference in between the two decay processes is the same as in the SM case. The leptons considered for the decay process are only electrons and muons, while the three neutrino flavours are considered, leading to a branching fraction $\mathcal{B}(\mathrm{hh} \to \mathrm{b\bar{b}VV} \to \mathrm{b\bar{b}l}\nu\mathrm{l}\nu)$

of 1.23%.

In the BSM scenario, 12 different shape benchmarks (BM) are defined to probe the parameter space of the 5 anomalous couplings described in the introduction. The benchmarks have been obtained, as described in [39], through a clustering procedure based on the distributions of di-Higgs invariant mass (m_{hh}) and cosine of the polar angle ($\cos\theta^{CS}_{hh}$) of one Higgs in the Collins-Soper frame [40]. This method is justified by the fact that at leading order and parton level, the signal can be characterized by only these two variables.

For all processes, the detector response is simulated using a detailed description of the CMS detector, based on the GEANT 4 package [41]. Additional simulated proton proton interactions via PYTHIA 8 are overlapped with the event of interest to reproduce the pileup measured in data.

3 Event selection and background predictions

Events are collected using a set of dilepton triggers, which require transverse momentum $p_T >$ 17 GeV for the first lepton and $p_T >$ 12 GeV (8 GeV) for the second electron (muon). Events with two oppositely charged leptons (e^+e^-, $\mu^+\mu^-$, $e^\pm\mu^\mp$) are selected, in which the electrons (muons) are required to have a p_T greater than 20 GeV and 15 GeV (10 GeV) for the higher and lower p_T lepton, respectively. Electrons (muons) in the pseudo-rapidity range $|\eta| < 2.5$ ($|\eta| < 2.4$) are considered. A dilepton mass requirement of $m_{ll} > 12$ GeV is applied in order to suppress quarkonia resonances.

Electrons, reconstructed by associating tracks with ECAL clusters, are identified by a cut-based selection using information on the cluster shape in the ECAL, track quality, and the matching between the track and the ECAL cluster [42]. Additionally, electrons from photon conversions are rejected. Muons are reconstructed from tracks found in the muon system, associated to tracks in the silicon tracking detectors [43]. They are identified based on the quality of the track fit and the number of associated hits in the different tracking detectors [43]. For both lepton flavours, the impact parameter with respect to the primary vertex has to be below 0.5 mm in the transverse plane and 1 mm along the beam direction. The lepton isolation, defined as the scalar p_T sum of all particle candidates in a cone around the lepton, excluding the lepton, divided by the lepton p_T, is required to be < 0.04 (< 0.15) for electrons (muons). Lepton identification efficiencies in the simulation are corrected for residual differences in between data and simulation.

Jets are reconstructed using a particle flow (PF) technique [44]. Candidates are clustered to form jets using the anti-k_T clustering algorithm [45], implemented in the FASTJET package [46], with a distance parameter of 0.4. Jet energies are corrected for residual non uniformity and non linearity of the detector response using corrections found with collision data [47]. Jets are required to have $p_T > 20$ GeV, $|\eta| < 2.4$, and be separated from identified leptons by a distance of $\sqrt{\Delta\phi^2 + \Delta\eta^2} = \Delta R > 0.3$. The magnitude of the negative vector sum of all PF candidates is referred to as E_T^{miss}. Corrections to the jet energy are propagated to the E_T^{miss}.

To identify jets originating from b quarks, the combined secondary vertex algorithm is used. Jets are considered as b-tagged if they pass the medium working point of the algorithm, which provides around 70% efficiency with a mistag rate less than 1%. Correction factors are applied to the selected jets in simulation to account for the different response of the combined secondary vertex algorithm in between data and simulation [48].

Among all possible dijet combinations fulfilling the previous criteria we select the two jets with

the highest combined secondary vertex outputs.

After the final object selection consisting of two opposite sign leptons and two b-tagged jets, a cut on $m_{ll} < m_Z - 15$ GeV is applied to remove the resonant Z peak and the high-m_{ll} tail of the Drell-Yan+jets and $t\bar{t}$ background processes. Fig. 2 shows the transverse momemtum of the dilepton system (p_T^{ll}) and the transverse momemtum of the dijet system (p_T^{jj}) distributions for data and simulated events after requiring all the cuts described in this section.

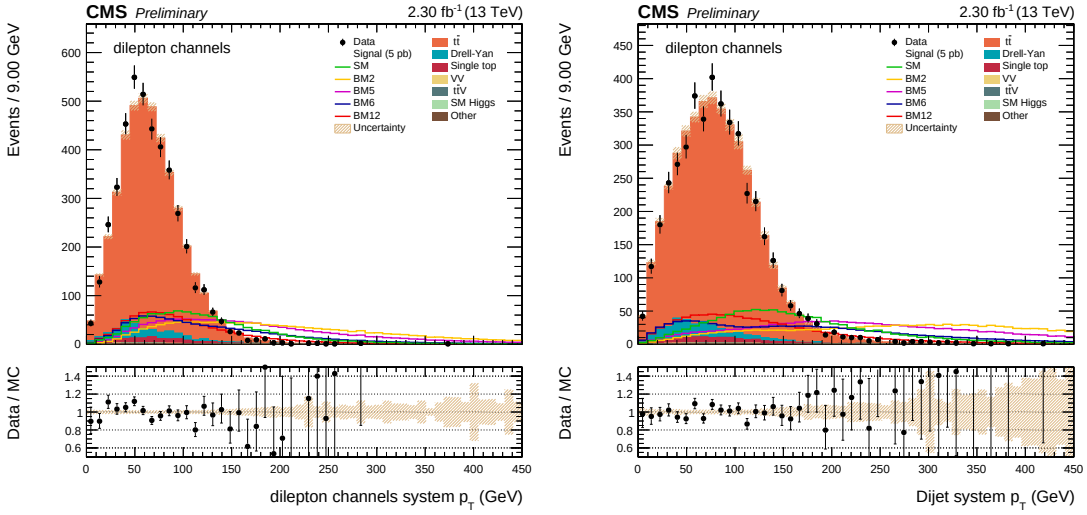

Figure 2: The p_T^{ll} (left) and p_T^{jj} (right) distributions for data and simulated events after requiring two leptons, two b-tagged jets, and $m_{ll} < m_Z - 15$ GeV, for all dilepton channels (ee, eμ, μe and $\mu\mu$). Four BMs along with the SM signal are shown as solid lines. The signal cross-sections times branching fraction are arbitrarily normalized to 5 pb for display purposes. Hashed area corresponds to postfit uncertainties, as described in section 6.

4 Signal extraction

A boosted decision tree (BDT) discriminant is used to improve the signal-to-background separation. The BDT utilizes information related to object kinematics and handles the correlations among them. In a phase space dominated by $t\bar{t}$ production, the variables provided as input to the BDT exploit the presence in the signal of two Higgs bosons decaying into two b-jets on the one hand, and two leptons and two neutrinos on the other hand, resulting in different kinematics for the di-lepton and di-jet systems between signal and background processes. The set of variables used as input is: m_{ll}, ΔR_{ll}, ΔR_{jj}, $\Delta\phi_{ll,jj}$, defined as the $\Delta\phi$ between the di-jet and the di-lepton systems, p_T^{ll}, p_T^{jj}, $\min(\Delta R_{j,l})$, and M_T, defined as $M_T = \sqrt{2p_T^{ll}E_T^{miss}(1-\cos(\Delta\phi(ll, E_T^{miss})))}$. The m_{jj} distribution is not used as BDT input in order to define a signal depleted control region, in the off-peak m_{jj} side bands. However, the m_{jj} distribution is used in combination with the BDT output as final discriminant, as described later. This set of BDT inputs was used in previous CMS studies targeting resonant di-Higgs searches in the same topology [49].

Due to the lack of statistics in the final regions the analysis is not split in different lepton flavours. As a consequence, all lepton channels (e^+e^-, $\mu^+\mu^-$, $e^\pm\mu^\mp$) are merged during BDT training. The dominant SM processes in the selection, namely $t\bar{t}$, Drell-Yan and single top, are considered as background.

A subset of four of the 12 BSM shape benchmarks have been selected and are shown in Fig. 2, 3 and 4 along with the SM case. These four samples (BM2, BM5, BM6, and BM12) correspond to different variations in the signal kinematics, which are driven by the shape of m_{hh}: single-mode soft (BM12) and hard (BM5) spectrum, as well as double-mode soft (BM6) and hard (BM2) spectrum. Different strategies were studied, considering either one of the chosen BMs or the SM sample as signal target to BDT training. It was found that using a BDT trained with BM2 leads to an optimal expected sensitivity for all 12 BMs and the SM. Therefore, the BDT trained with BM2 is used as the only signal vs. background discriminant in the analysis. In order to set limits on different points of the BSM parameter space, the simulated BSM samples are reweighted using parton-level distributions of m_{hh} vs. $\cos\theta^{CS}_{hh}$ obtained for 1459 different sets of anomalous coupling values.

The BDT discriminant and m_{jj} distributions after selection cuts are shown in Fig. 3. Given their discrimination power between signal and background, both distributions are combined to enhance the sensitivity of the analysis. We define three regions in m_{jj}: two of them enriched in background, $m_{jj} < 75$ GeV and $m_{jj} \geq 140$ GeV, and the other enriched in signal, $m_{jj} \in [75, 140[$. For each region, we use the BDT output as our final discriminant, as shown in Fig. 4, where the three m_{jj} regions are represented in a single distribution.

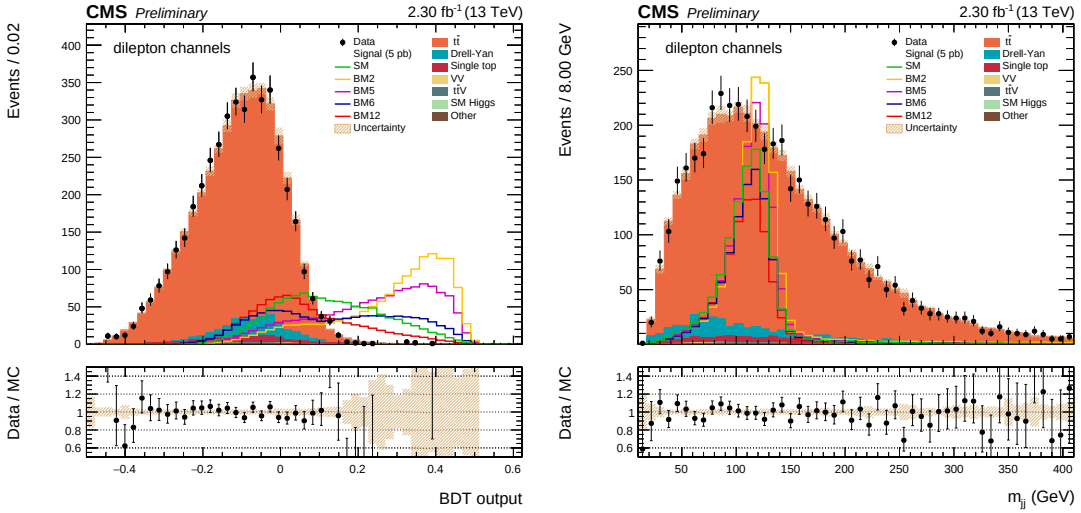

Figure 3: The BDT output (left) and m_{jj} (right) distributions for data and simulated events for all dilepton channels (ee, eμ, μe and $\mu\mu$) after requiring all selection cuts. Four BMs along with the SM signal are shown as solid lines. The signal cross-sections times branching fraction are arbitrarily normalized to 5 pb. Hashed area corresponds to postfit uncertainties, as described in section 6.

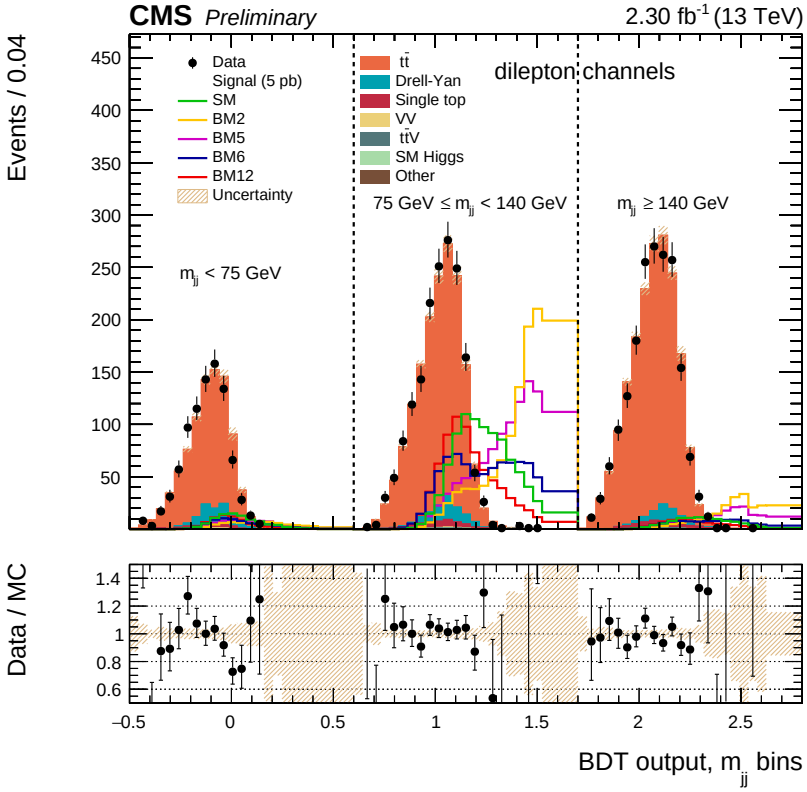

Figure 4: BDT output distribution for data and simulated events for all dilepton channels (ee, eμ, μe and $\mu\mu$) in three different m_{jj} regions: $m_{jj} < 75$ GeV (left), $m_{jj} \in [75, 140[$ GeV (middle) and $m_{jj} \geq 140$ GeV (right). Four BMs along with the SM signal are shown as solid lines. The signal cross-sections times branching fraction are arbitrarily normalized to 5 pb. Hashed area corresponds to postfit uncertainties, as described in section 6.

5 Systematic uncertainties

This analysis depends on both normalization and shape of the background and signal expectations. We investigate sources of systematic uncertainties and their effect on the final statistical interpretation of the results by considering both uncertainties in the normalization, or rate, of the various processes in the analysis, as well as those that change the shape of the distributions.

Theoretical uncertainties on the cross section used to predict the $\mathrm{t\bar{t}}$, Drell-Yan and single top backgrounds are considered as systematic uncertainties on the yield estimates. The uncertainty on the total integrated luminosity is determined to be 2.7% [50].

We consider the following sources of systematic uncertainties which affect the normalization and shape of the templates used in the statistical evaluation:

- **Lepton identification and isolation**: Uncertainties on the electrons and muons isolation and identification are determined and provided centrally, extracted with a "tag-and-probe" analysis on $\mathrm{Z} \to \mathrm{ll}$ events.
- **Jet energy scale and resolution**: Uncertainties in the jet energy scale are of the order of a few percent as a function of jet p_{T} and η. We vary the jet energy scale by $\pm 1\,\sigma$. A difference in the jet energy resolution of about 10% between data and simulation is accounted for by worsening the jet energy resolution in the simulation by η-dependent factors. The uncertainty on these corrections is estimated by a variation of the factors applied by $\pm 1\,\sigma$. These variations in jet energies are propagated to the $E_{\mathrm{T}}^{\mathrm{miss}}$.
- **Trigger efficiency**: Trigger efficiencies are evaluated using the "tag-and-probe" technique. Uncertainties on this measurement are considered as a source of systematic uncertainty.
- **b-tagging**: B-tag and mistag rate corrections are determined as a function of the jet p_{T} and η. Their effect on the analysis is estimated by varying these corrections by one standard deviation.
- **Pile-up**: The measured minimum-bias cross section is varied by $\pm 5\%$ to produce different expected pileup distributions.
- **QCD scale uncertainty**: This uncertainty is estimated by varying the renormalization (μ_R) and the factorization (μ_F) scales, used during the MC generation of the sample, independently by a factor 0.5, 1 or 2. Unphysical cases, where one scale fluctuate up while the other fluctuate down, are not considered. An envelope is built from all the 6 possible variations by keeping, for each bin of the distributions, its maximum and minimum variations, and is used as an estimate of the QCD scale uncertainties for all the background and signal samples.
- **Parton Distribution Functions (PDFs) uncertainty**: The magnitude of the uncertainties related to the parton distribution functions and the variation of the strong coupling constant for each simulated background and signal processes is obtained using replicas of the NNPDF 3.0 set [51].
- **MC statistics**: We consider as an additional source of systematic uncertainties the finite nature of simulation samples. For each bin of the distributions, one additional uncertainty is added, where only the considered bin is variated by $\pm 1\,\sigma$, fixing the others to their nominal value.

The effects on the total yields in the final region are summarized in Table 1.

Table 1: Summary of the systematic uncertainties and their impact range on total background yields and on the SM signal in the final region.

Source	Background yield variation	SM signal yield variation
Jet b-tagging	3.6%	3.5%
Trigger efficiency	3.3%	4.0%
Luminosity	2.7%	2.7%
Jet energy scale	1.7%	1.4%
Muon ID	1.2%	1.2%
Muon ISO	0.9%	0.7%
Parton distributions	0.6%	0.2%
Electron ID & ISO	0.5%	0.5%
Pileup	0.2%	0.2%
Jet energy resolution	$< 0.1\%$	$< 0.1\%$
Affecting only $t\bar{t}$ (90.7% of the total bkg.)		
QCD scale	12.9%	
$t\bar{t}$ cross-section	5.2%	
MC stat.	$< 0.1\%$	
Affecting only Drell-Yan (6.0% of the total bkg.)		
QCD scale	15.2%	
Drell-Yan cross-section	4.9%	
MC stat.	4.5%	
Affecting only Single top (2.6% of the total bkg.)		
Single top cross-section	7.0%	
MC stat.	0.7%	
QCD scale	0.3%	
Affecting only SM signal		
QCD scale	24.3%	
MC stat.	$< 0.1\%$	

6 Results

We first perform a binned maximum likelihood fit in order to extract best-fit signal cross sections, where all the nuisances parameters described in section 5 are free to float. The fit is performed using templates built from BDT output distributions in three m_{jj} regions, as shown in Fig. 4. The likelihood function is the product of the Poisson likelihoods over all bins of the templates and is given by

$$L(\beta_{\text{signal}}, \beta_k|\text{data}) = \prod_{i=1}^{N_{\text{bins}}} \frac{\mu_i^{n_i} \cdot e^{-\mu_i}}{n_i!}$$

where n_i is the number of observed events in bin i and the Poisson mean for bin i is given by

$$\mu_i = \beta_{\text{signal}} \cdot S_i + \sum_k \beta_k \cdot T_{k,i},$$

where k denotes all of the considered background processes, $T_{k,i}$ is the bin content of bin i of the template for process k and S_i is the bin content of bin i of the signal template. The parameter β_k is the nuisance parameter for the normalization of the process k and β_{signal} is the signal strength.

The simulated background templates are scaled to the data luminosity, according to theoretical cross sections. The signal templates are also normalized to the data luminosity, but considering a cross section of 1 fb. This allows to reinterpret β_{signal} directly as the signal cross section in fb. For each systematic uncertainty, a nuisance parameter δ_u is introduced with a log-normal prior which modifies μ_i, to describe the yield variation induced by the considered systematics in each bin of the templates.

The fit results in signal cross sections compatible with zero: no significant excess above background predictions is seen. We therefore proceed to set upper limits at 95% confidence level (CL) on Higgs pair production cross section times branching fraction for $hh \to b\bar{b}VV \to b\bar{b}l\nu l\nu$ using the asymptotic modified frequentist method (asymptotic CL_s) [52, 53]. The upper limit on SM $hh \to b\bar{b}VV \to b\bar{b}l\nu l\nu$ cross section is found to be 166.7 ($92.8^{+59.9}_{-33.4}$) fb. Including theoretical uncertainties on the SM signal cross section, this limit amounts to 410 (227^{+147}_{-82}) times the SM prediction. In the BSM hypothesis, upper limits are set as a function of κ_λ and κ_t, as shown in Fig. 5. Figure 6 shows excluded and allowed values of the BSM couplings in the κ_λ vs κ_t plane for two sets of BSM coupling values. Upper limits as a function of the other considered couplings, c_2, c_g and c_{2g} are available as supplementary material[1].

In order to estimate postfit uncertainties, we perform a binned maximum likelihood fit of the mjj vs. BDT output distributions (Fig. 4) to the data, extracting the best-fit values for all the nuisance parameters. This fit is performed in the background-only hypothesis, for which only nuisance parameters affecting the backgrounds are considered. Postfit uncertainties are estimated from random variations of all the nuisance parameters, sampled from the fit result's covariance matrix.

7 Summary

We have presented a search for Higgs boson pair production, hh, where one of the h decays as $h \to b\bar{b}$, and the other as $h \to VV \to l\nu l\nu$, using LHC proton-proton collision data at

[1] http://cms-results.web.cern.ch/cms-results/public-results/preliminary-results/HIG-16-024/index.html

$\sqrt{s}$ = 13 TeV corresponding to an integrated luminosity of 2.30 fb^{-1}. Data and standard model predictions are in agreement within uncertainties. For the SM hh hypothesis, the data are observed (expected) to exclude a production cross section times branching ratio of 166.7 ($92.8^{+59.9}_{-33.4}$) fb, corresponding to approximately 400 times the SM cross section. Searching for deviations from the SM, upper limits are set on hh $\rightarrow$ b$\bar{\text{b}}$VV $\rightarrow$ b$\bar{\text{b}}$lνlν cross section in scenarios considering five anomalous couplings: κ_λ, κ_t, c_2, c_g, and c_{2g}.

The search for Higgs boson pair production in the b$\bar{\text{b}}$lνlν final state is performed for the first time using LHC data. With the present luminosity, the analysis is insensitive to SM hh production but is already excluding some regions of the BSM parameter space.

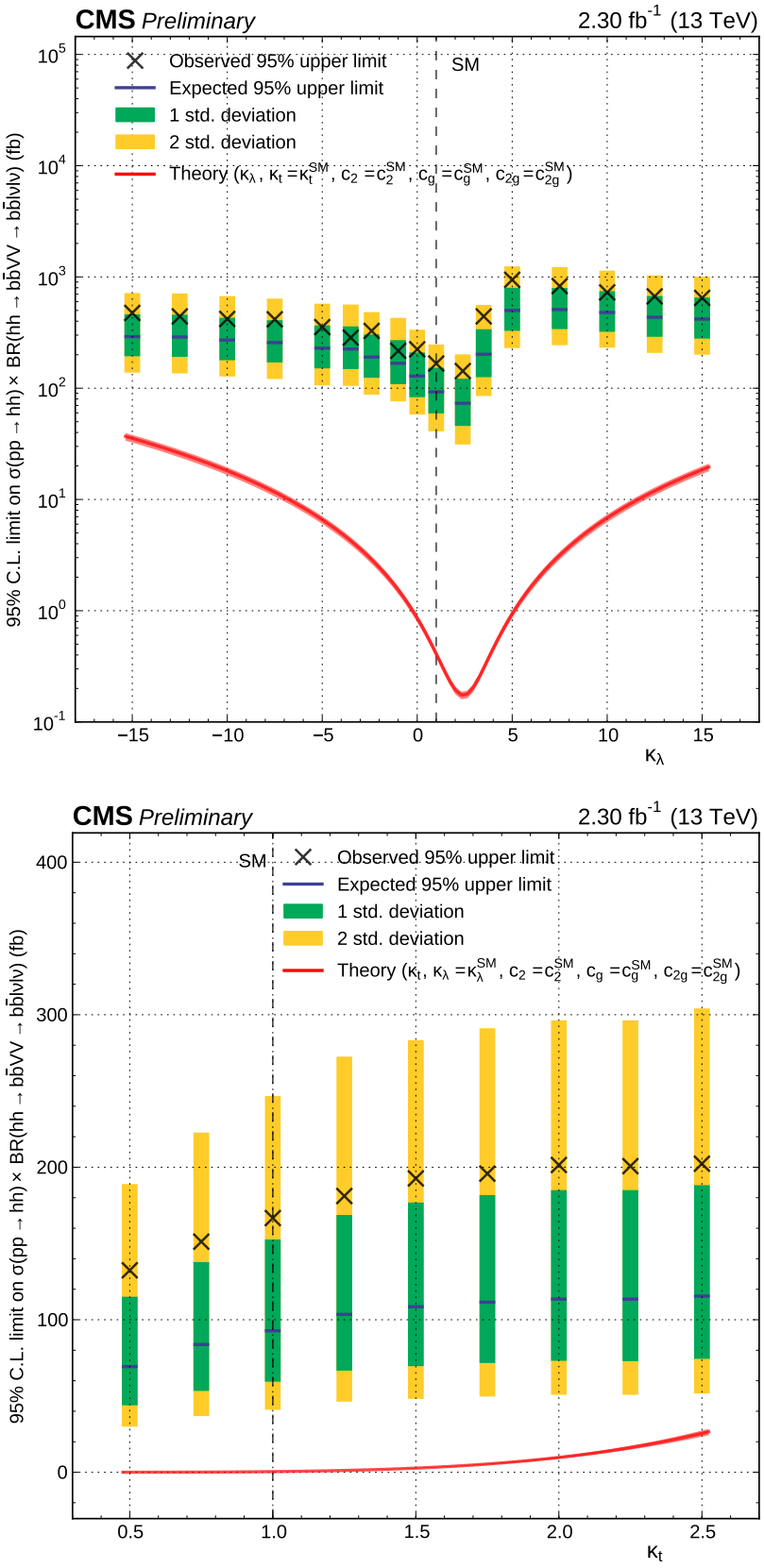

Figure 5: Expected and observed 95% CL upper limits on the Higgs pair production cross section times branching fraction for hh $\rightarrow$ bb̄VV $\rightarrow$ bb̄lνlν as a function of κ_λ (top) and κ_t (bottom). The κ_λ (κ_t) scans are performed assuming $c_2 = 0$, $c_g = 0$, and $c_{2g} = 0$, while $\kappa_t = 1$ ($\kappa_\lambda = 1$). These limits are computed using the asymptotic CL$_s$ method. Theory predictions are extracted from [9–14, 54].

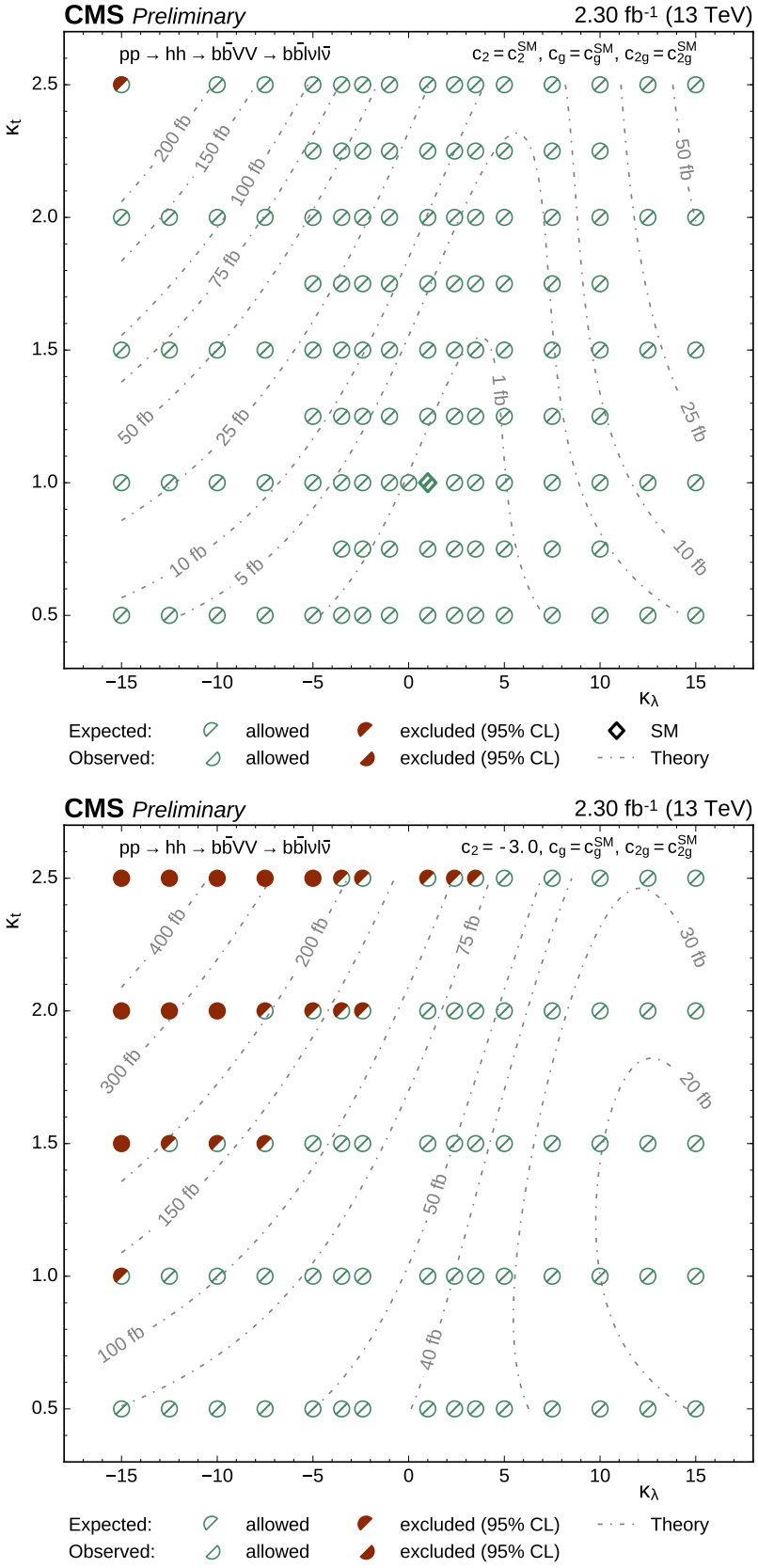

Figure 6: Allowed (empty half-circles) and excluded (solid half-circles) points of the BSM parameter space at expected and observed 95% CL in the κ_λ vs κ_t plane. Theoretical cross-section times branching fraction isolines for hh $\to$ b$\bar{\text{b}}$VV $\to$ b$\bar{\text{b}}$lνlν are shown as dashed lines. Other BSM couplings are set to their (null) SM value in the upper figure, and to $c_2 = -3$, $c_g = 0$, and $c_{2g} = 0$ in the bottom figure. The limits are computed using the asymptotic CL_s method. Theory predictions are extracted from [9–14, 54].

References

[1] F. Englert and R. Brout, "Broken Symmetry and the Mass of Gauge Vector Mesons", *Phys. Rev. Lett.* **13** (1964) 321, doi:10.1103/PhysRevLett.13.321.

[2] P. W. Higgs, "Broken symmetries, massless particles and gauge fields", *Phys. Lett.* **12** (1964) 132, doi:10.1016/0031-9163(64)91136-9.

[3] P. W. Higgs, "Broken Symmetries and the Masses of Gauge Bosons", *Phys. Rev. Lett.* **13** (1964) 508, doi:10.1103/PhysRevLett.13.508.

[4] G. S. Guralnik, C. R. Hagen, and T. W. B. Kibble, "Global conservation laws and massless particles", *Phys. Rev. Lett.* **13** (1964) 585, doi:10.1103/PhysRevLett.13.585.

[5] P. W. Higgs, "Spontaneous symmetry breakdown without massless bosons", *Phys. Rev.* **145** (1966) 1156, doi:10.1103/PhysRev.145.1156.

[6] T. W. B. Kibble, "Symmetry breaking in non-Abelian gauge theories", *Phys. Rev.* **155** (1967) 1554, doi:10.1103/PhysRev.155.1554.

[7] ATLAS Collaboration, "Observation of a new particle in the search for the Standard Model Higgs boson with the ATLAS detector at the LHC", *Phys.Lett. B* **716** (2012) 129.

[8] CMS Collaboration, "Observation of a new boson at a mass of 125 GeV with the CMS experiment at the LHC", *Phys.Lett. B* **716** (2012) 3061.

[9] B. Mellado Garcia, P. Musella, M. Grazzini, and R. Harlander, "CERN Report 4: Part I Standard Model Predictions", LHCHXSWG-DRAFT-INT- 2016-008, 2016.

[10] D. de Florian and J. Mazzitelli, "Higgs pair production at next-to-next-to-leading logarithmic accuracy at the LHC", *JHEP* **09** (2015) 053, doi:10.1007/JHEP09(2015)053, arXiv:1505.07122.

[11] D. de Florian and J. Mazzitelli, "Higgs Boson Pair Production at Next-to-Next-to-Leading Order in QCD", *Phys. Rev. Lett.* **111** (2013) 201801, doi:10.1103/PhysRevLett.111.201801, arXiv:1309.6594.

[12] S. Borowka et al., "Higgs boson pair production in gluon fusion at NLO with full top-quark mass dependence", arXiv:1604.06447.

[13] S. Dawson, S. Dittmaier, and M. Spira, "Neutral Higgs boson pair production at hadron colliders: QCD corrections", *Phys. Rev.* **D58** (1998) 115012, doi:10.1103/PhysRevD.58.115012, arXiv:hep-ph/9805244.

[14] J. Grigo, K. Melnikov, and M. Steinhauser, "Virtual corrections to Higgs boson pair production in the large top quark mass limit", *Nucl.Phys.* **B888** (2014) 17–29, doi:10.1016/j.nuclphysb.2014.09.003, arXiv:1408.2422.

[15] J. Grigo, J. Hoff, and M. Steinhauser, "Higgs boson pair production: top quark mass effects at NLO and NNLO", *Nucl. Phys.* **B900** (2015) 412–430, doi:10.1016/j.nuclphysb.2015.09.012, arXiv:1508.00909.

[16] J. Grigo, J. Hoff, K. Melnikov, and M. Steinhauser, "On the Higgs boson pair production at the LHC", *Nucl. Phys.* **B875** (2013) 1–17, doi:10.1016/j.nuclphysb.2013.06.024, arXiv:1305.7340.

[17] R. Frederix et al., "Higgs pair production at the LHC with NLO and parton-shower effects", *Phys. Lett.* **B732** (2014) 142–149, doi:10.1016/j.physletb.2014.03.026, arXiv:1401.7340.

[18] F. Maltoni, E. Vryonidou, and M. Zaro, "Top-quark mass effects in double and triple Higgs production in gluon-gluon fusion at NLO", *JHEP* **11** (2014) 079, doi:10.1007/JHEP11(2014)079, arXiv:1408.6542.

[19] A. Azatov, R. Contino, G. Panico, and M. Son, "Effective field theory analysis of double Higgs boson production via gluon fusion", *Phys. Rev.* **D92** (2015), no. 3, 035001, doi:10.1103/PhysRevD.92.035001, arXiv:1502.00539.

[20] F. Goertz, A. Papaefstathiou, L. L. Yang, and J. Zurita, "Higgs boson pair production in the D=6 extension of the SM", *JHEP* **04** (2015) 167, doi:10.1007/JHEP04(2015)167, arXiv:1410.3471.

[21] B. Hespel, D. Lopez-Val, and E. Vryonidou, "Higgs pair production via gluon fusion in the Two-Higgs-Doublet Model", *JHEP* **09** (2014) 124, doi:10.1007/JHEP09(2014)124, arXiv:1407.0281.

[22] CMS Collaboration, "Search for two Higgs bosons in final states containing two photons and two bottom quarks", Technical Report CERN-EP-2016-050. CMS-HIG-13-032-003. arXiv:1603.06896, CERN, Geneva, Mar, 2016. Comments: Submitted to Phys. Rev. D.

[23] CMS Collaboration, "Search for non-resonant Higgs boson pair production in the $b\bar{b}\tau^+\tau^-$ final state", Technical Report CMS-PAS-HIG-16-012, CERN, Geneva, 2016.

[24] CMS Collaboration, "Model independent search for Higgs boson pair production in the $b\bar{b}\tau^+\tau^-$ final state", Technical Report CMS-PAS-HIG-15-013, CERN, Geneva, 2016.

[25] ATLAS Collaboration, "Search For Higgs Boson Pair Production in the $\gamma\gamma b\bar{b}$ Final State using pp Collision Data at $\sqrt{s} = 8$ TeV from the ATLAS Detector", *Phys. Rev. Lett.* **114** (2015), no. 8, 081802, doi:10.1103/PhysRevLett.114.081802, arXiv:1406.5053.

[26] ATLAS Collaboration, "Search for Higgs boson pair production in the $b\bar{b}b\bar{b}$ final state from pp collisions at $\sqrt{s} = 8$ TeVwith the ATLAS detector", *Eur. Phys. J.* **C75** (2015), no. 9, 412, doi:10.1140/epjc/s10052-015-3628-x, arXiv:1506.00285.

[27] ATLAS Collaboration, "Searches for Higgs boson pair production in the $hh \to bb\tau\tau, \gamma\gamma WW^*, \gamma\gamma bb, bbbb$ channels with the ATLAS detector", *Phys. Rev.* **D92** (2015) 092004, doi:10.1103/PhysRevD.92.092004, arXiv:1509.04670.

[28] ATLAS Collaboration, "Search for pair production of Higgs bosons in the $b\bar{b}b\bar{b}$ final state using proton–proton collisions at $\sqrt{s} = 13$ TeV with the ATLAS detector", arXiv:1606.04782.

[29] ATLAS Collaboration, "Search for Higgs boson pair production in the $b\bar{b}\gamma\gamma$ final state using pp collision data at $\sqrt{s} = 13$ TeV with the ATLAS detector", Technical Report ATLAS-CONF-2016-004, CERN, Geneva, Mar, 2016.

[30] CMS Collaboration, "The CMS experiment at the CERN LHC", *JINST* **0803** (2008) S08004.

[31] J. Alwall et al., "The automated computation of tree-level and next-to-leading order differential cross sections, and their matching to parton shower simulations", *JHEP* **07** (2014) 079, doi:10.1007/JHEP07(2014)079, arXiv:1405.0301.

[32] P. Nason, "A New method for combining NLO QCD with shower Monte Carlo algorithms", *JHEP* **11** (2004) 040, doi:10.1088/1126-6708/2004/11/040, arXiv:hep-ph/0409146.

[33] S. Frixione, P. Nason, and C. Oleari, "Matching NLO QCD computations with Parton Shower simulations: the POWHEG method", *JHEP* **11** (2007) 070, doi:10.1088/1126-6708/2007/11/070, arXiv:0709.2092.

[34] S. Alioli, P. Nason, C. Oleari, and E. Re, "A general framework for implementing NLO calculations in shower Monte Carlo programs: the POWHEG BOX", *JHEP* **06** (2010) 043, doi:10.1007/JHEP06(2010)043, arXiv:1002.2581.

[35] S. Alioli, S. Moch, and P. Uwer, "Hadronic top-quark pair-production with one jet and parton showering", *JHEP* **1201** (2012) 137.

[36] S. Alioli, P. Nason, C. Oleari, and E. Re, "Single-top production in the s- and t-channel", *JHEP* **0909** (2009) 111.

[37] T. Sjostrand, S. Mrenna, and P. Z. Skands, "PYTHIA 6.4 Physics and Manual", *JHEP* **05** (2006) 026, doi:10.1088/1126-6708/2006/05/026, arXiv:hep-ph/0603175.

[38] T. Sjostrand, S. Mrenna, and P. Z. Skands, "A Brief Introduction to PYTHIA 8.1", *Comput. Phys. Commun.* **178** (2008) 852–867, doi:10.1016/j.cpc.2008.01.036, arXiv:0710.3820.

[39] A. Carvalho et al., "Higgs Pair Production: Choosing Benchmarks With Cluster Analysis", *JHEP* **04** (2016) 126, doi:10.1007/JHEP04(2016)126, arXiv:1507.02245.

[40] J. C. Collins and D. E. Soper, "Angular distribution of dileptons in high-energy hadron collisions", *Phys. Rev. D* **16** (Oct, 1977) 2219–2225, doi:10.1103/PhysRevD.16.2219.

[41] S. Agostinelli et al., "Geant4a simulation toolkit", *Nuclear Instruments and Methods in Physics Research Section A: Accelerators, Spectrometers, Detectors and Associated Equipment* **506** (2003), no. 3, 250 – 303, doi:http://dx.doi.org/10.1016/S0168-9002(03)01368-8.

[42] CMS Collaboration, "Performance of electron reconstruction and selection with the CMS detector in proton-proton collisions at $\sqrt{s}$ = 8 TeV", *JINST* **10** (2015), no. 06, P06005, doi:10.1088/1748-0221/10/06/P06005, arXiv:1502.02701.

[43] CMS Collaboration, "Performance of CMS muon reconstruction in pp collision events at $\sqrt{s} = 7$ TeV", *JINST* **7** (2012) P10002, doi:10.1088/1748-0221/7/10/P10002, arXiv:1206.4071.

[44] CMS Collaboration, "Performance of the CMS missing transverse momentum reconstruction in pp data at $\sqrt{s}$ = 8 TeV", *JINST* **10** (2015) P02006.

[45] M. Cacciari, G. P. Salam, and G. Soyez, "The anti-k_T jet clustering algorithm", *JHEP* **04** (2008) 063.

[46] M. Cacciari, G. P. Salam, and G. Soyez, "FastJet user manual", *Eur. Phys. J. C* **72** (2012) 1896.

[47] CMS Collaboration, "Jet Energy Calibration in the 8 TeV pp data", *CMS-PAS-JME-13-004* **2015**.

[48] CMS Collaboration, "Identification of b-quark jets with the CMS experimet", *JINST* **8** (2013) P04013.

[49] CMS Collaboration, "Search for resonant Higgs boson pair production in the $b\bar{b}l\nu l\nu$ final state at $\sqrt{s} = 13$ TeV", *CMS-PAS-HIG-16-011* (2016).

[50] CMS Collaboration, "CMS Luminosity Measurement for the 2015 Data Taking Period", Technical Report CMS-PAS-LUM-15-001, CERN, Geneva, 2016.

[51] NNPDF Collaboration, "Parton distributions for the LHC Run II", *JHEP* **04** (2015) 040, doi:10.1007/JHEP04(2015)040, arXiv:1410.8849.

[52] T. Junk, "Confidence level computation for combining searches with small statistics", *Nucl.Instrum.Meth.* **A434** (1999) 435, doi:10.1016/S0168-9002(99)00498-2, arXiv:hep-ex/9902006.

[53] A. L. Read, "Presentation of search results: the CLs technique", *J. Phys. G: Nucl. Part. Phys.* **28** (2002).

[54] A. Carvalho Antunes De Oliveira et al., "Analytical parametrization and shape classification of anomalous HH production in EFT approach", Technical Report LHCHXSWG-2016-001, CERN, Geneva, Jul, 2016.